Environmental Science & Technology

pubs.acs.org/est

Article

Coexisting Goethite Promotes Fe(II)-Catalyzed Transformation of Ferrihydrite to Goethite

Luiza Notini,* Laurel K. ThomasArrigo, Ralf Kaegi, and Ruben Kretzschmar

Cite This: *Environ. Sci. Technol.* 2022, 56, 12723−12733

Read Online

ACCESS | Metrics & More | Article Recommendations | Supporting Information

ABSTRACT: In redox-affected soil environments, electron transfer between aqueous Fe(II) and solid-phase Fe(III) catalyzes mineral transformation and recrystallization processes. While these processes have been studied extensively as independent systems, the coexistence of iron minerals is common in nature. Yet it remains unclear how coexisting goethite influences ferrihydrite transformation. Here, we reacted ferrihydrite and goethite mixtures with Fe(II) for 24 h. Our results demonstrate that with more goethite initially present in the mixture more ferrihydrite turned into goethite. We further used stable Fe isotopes to label different Fe pools and probed ferrihydrite transformation in the presence of goethite using ^{57}Fe Mössbauer spectroscopy and changes in the isotopic composition of solid and aqueous phases. When ferrihydrite alone underwent Fe(II)-catalyzed transformation, Fe atoms initially in the aqueous phase mostly formed lepidocrocite, while those from ferrihydrite mostly formed goethite. When goethite was initially present, more goethite was formed from atoms initially in the aqueous phase, and nanogoethite formed from atoms initially in ferrihydrite. Our results suggest that coexisting goethite promotes formation of more goethite via Fe(II)−goethite electron transfer and template-directed nucleation and growth. We further hypothesize that electron transfer onto goethite followed by electron hopping onto ferrihydrite is another possible pathway to goethite formation. Our findings demonstrate that mineral transformation is strongly influenced by the composition of soil solid phases.

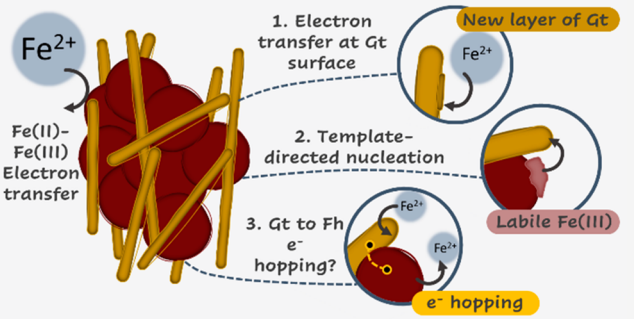

KEYWORDS: *Fe(II)−Fe(III) electron transfer, recrystallization, template-directed nucleation, labile Fe(III), electron hopping*

INTRODUCTION

Ferrihydrite is a short-range ordered iron (Fe) oxyhydroxide typically formed via Fe(III) hydrolysis and is therefore widely distributed in soils and sediments.[1] Due to its high specific surface area, ferrihydrite plays an essential role in biogeochemical cycles, serving as a bioavailable form of Fe(III) and a sorbent phase for nutrients and contaminants.[2,3] Goethite is a prevalent product of the transformation of ferrihydrite, and due to its high thermodynamic stability, is one of the most common iron oxides in soils, being found in both aerobic and anaerobic soils and sediments.[1,4]

Under anoxic conditions, ferrihydrite and goethite can react with microbially derived aqueous Fe(II), and the reactions of the Fe(II)−Fe(III) redox couple will catalyze changes in the minerals. Upon reaction with Fe(II), ferrihydrite undergoes Fe(II)−Fe(III) electron transfer[5] and exchanges Fe atoms in the aqueous and solid phase.[6,7] This reaction leads to Fe(II)-catalyzed transformations into lepidocrocite, goethite, and magnetite, depending on Fe(II) concentrations,[8,9] pH,[10] and the presence of ligands[7,8,11] or trace elements.[12−17] Several mechanisms have been proposed to explain the Fe(II)-catalyzed transformation of ferrihydrite, including dissolution/reprecipitation, internal rearrangement within particle aggregates, and particle-based recrystallization.[18] Recent studies highlight the possible role of a labile Fe(III) species. According to this hypothesis, the Fe(II) that sorbs onto ferrihydrite undergoes electron transfer[7,19] and forms a labile Fe(III) species which is more soluble than the original ferrihydrite.[21] The buildup of labile Fe(III) is thought to be responsible for accelerated nucleation and growth of lepidocrocite and goethite via Fe(III) dissolution/reprecipitation.[21−23] While the solubility of Fe(III) at circumneutral pH is very low, in situ transmission electron microscopy studies have recorded the dissolution of individual ferrihydrite aggregates in the presence of Fe(II).[24,25]

For goethite, a thermodynamically more stable mineral than ferrihydrite, Fe(II)−goethite electron transfer leads to mineral

Received: May 31, 2022
Revised: August 8, 2022
Accepted: August 9, 2022
Published: August 23, 2022

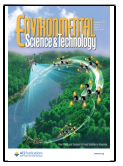

recrystallization, with the exchange of Fe atoms between solids and solution, despite no formation of new mineral phases.[5,19,26,27] Previous works have found that mineral surface defects can be a driving force for Fe(II)−goethite electron transfer,[28−30] and that the accumulation of Fe(II) sorbed onto the mineral surface might slow the process over time.[31,32] In addition, Fe(II)−goethite electron transfer is affected by pH,[33] anions,[34] and the presence of trace metals.[34] While a previous study reported no changes in goethite morphology,[19] others have indicated changes in length to width ratio and morphology of the recrystallized mineral.[35,36] Note that most studies on the transformation and recrystallization of Fe minerals at circumneutral pH values have employed MOPS buffer,[11,13,37,38] HEPES buffer,[23,28,31] or PIPES buffer.[21,23] However, MOPS buffer and HEPES buffer have impacts on the surface chemistry and, therefore, redox reactions,[39] while PIPES buffer impacts the amount of Fe(II) released from the ferrihydrite.[21] Nonetheless, Fe mineral transformation and electron transfer between aqueous Fe(II) and Fe(III) minerals have been demonstrated in buffered and unbuffered systems.[21,28] Therefore, while the phenomena investigated in this work can be affected by the choice of buffers, they are not an artifact of the use of buffers.

While abundant literature describes how ferrihydrite and goethite react with Fe(II) separately, these minerals are commonly found together in natural systems,[1] from Fe-rich flocs in the wetlands of Iceland,[40] to agricultural soils in the Netherlands,[41] to forest soils in Russia.[42] However, little is known about how coexisting minerals will affect their transformation in anoxic environments. We hypothesize that coexisting goethite will affect the Fe(II)-catalyzed transformation of ferrihydrite by providing a template for nucleation and growth of more goethite. Therefore, we investigated how and to what extent the coexistence of goethite affects Fe(II)-catalyzed ferrihydrite transformation and the fate of Fe atoms in solution and solid phases. We used stable Fe isotopes (^{54}Fe, ^{56}Fe, ^{57}Fe) to label the Fe atoms from different initial pools (ferrihydrite, goethite, and Fe(II)) and probed the reaction using ^{57}Fe Mössbauer spectroscopy and the isotope composition of the solid and aqueous phases.

MATERIAL AND METHODS

Iron Mineral Synthesis. Ferrihydrite and nanometer-sized goethite were prepared from natural isotope-abundance iron metal powder (^{NA}Fe(0)) or ^{56}Fe(0) metal powder (Isoflex, 99.5% isotope purity). The synthesis started from zerovalent iron (Fe(0)) as opposed to commonly used Fe salts to allow for the use of commercially available isotope-labeled Fe(0). A similar approach has been used to synthesize ferrihydrite,[5] goethite,[43] magnetite,[44] and hematite.[45] For the synthesis of ferrihydrite, 300 mg of Fe(0) was dissolved in 30 mL of 2 M HCl (Normatom) to obtain an Fe(II) stock solution. This solution was then oxidized with excess H_2O_2 (35%, Merck) and subsequently filtered (0.22 μm, nylon, BGB). Then the pH of the Fe(III) solution was raised to pH 7−8 by dropwise adding 1 M KOH (MQ500, Merck) under constant stirring. Goethite was synthesized using a protocol adapted from Cwiertny and collaborators.[47] Briefly, an Fe(II) solution was prepared by dissolving 250 mg of Fe(0) in 50 mL of 0.2 M HCl. This solution was oxidized with excess H_2O_2 and subsequently filtered (0.22 μm, nylon, BGB). The pH of the Fe(III) solution was then adjusted to 1.9 by dropwise adding 1 M KOH under constant stirring. Then, using a peristaltic pump at a flow of 5 mL min^{-1}, 89 mL of a 60 mM sodium bicarbonate solution (Merck) was added to the Fe(III) suspension to achieve a final pH of 2.7. The resulting suspension was placed in closed Nalgene bottles, boiled using a microwave (800 W, ∼5 min), and immediately cooled to room temperature using an ice−water bath. The suspension was purified via dialysis (Spectrum Spectra, 3500 Da MWCO) for 3 days against ultrapure water (UPW, Milli-Q, Millipore, 18.2 MΩ·cm), which was replaced 3 times per day. The solution was then added to a Nalgene bottle, and the pH was raised to 13 by dropwise adding 5 M KOH under constant stirring. Finally, the bottle was closed and placed in an oven at 90 °C for 24 h.

After the synthesis of ferrihydrite and goethite, the resulting precipitates were centrifuged at 3500g for 25 min and washed with UPW multiple times until the conductivity was <100 μS cm^{-1}. Then the washed solids were resuspended in 50 mL of UPW. The suspensions were shock-frozen by dropwise injection into liquid N_2, freeze-dried, gently homogenized with a mortar and pestle, and stored in brown glass bottles in a desiccator until use. We synthesized ferrihydrite and goethite from ^{NA}Fe(0) and ^{56}Fe(0) (here referred to as ^{NA}Fh, ^{56}Fh, ^{NA}Gt, and ^{56}Gt), and X-ray diffraction (XRD) patterns confirmed that ferrihydrite or goethite were the only mineral phases formed (Figure S1). The specific surface area of the products was determined by multipoint N_2-BET analysis (Quantachrome) after 15 h of outgassing at 120 °C and was found to be 263 m^2 g^{-1} for ^{NA}Fe and 62 m^2 g^{-1} for ^{NA}Gt. The mineral isotopic compositions were determined as described below and are listed in Table S1.

Experimental Setup. All experiments were carried out in a glovebox under anoxic conditions (N_2 atmosphere, <5 ppm of O_2), and all solutions were purged for at least 2 h with N_2 (99.99% purity) prior to transfer into the glovebox. To prepare the Fe(II) spike solution, Fe(II) stock solutions were prepared by dissolving 89 mg of ^{NA}Fe(0) in 4.5 mL of 1 M HCl overnight. The resulting solution was filtered (0.22 μm, nylon, BGB) to remove residual Fe(0) and diluted to 15 mL with UPW.

In this study, we considered it crucial to avoid pH drifts to allow us to isolate the effect of the coexistence of goethite. Therefore, we chose to work with a MOPS buffer, which allows a direct comparison with similar studies.[11,13,37,38] While our results might be slightly affected by the use of MOPS, the fact that all reactions were conducted using the same buffer allows us to evaluate the effect of the coexistence of goethite in the transformation of ferrihydrite. Batch reactors were prepared in 50 mL crimp septum vials containing 45 mL of 50 mM MOPS (3-(*N*-morpholino)propanesulfonic acid) buffer adjusted to pH 7.0 ± 0.05 spiked with aliquots the Fe(II) stock solution to reach an initial concentration of 1 mM Fe(II). The initial concentration was confirmed using the 1,10-phenanthroline method[46] and is reported in Table S2.

The reaction was started by adding the desired Fe mineral(s) to reach a concentration of 10 mM of Fe(III) in the reactors and obtain an Fe(II):Fe(III) ratio of 1:10. The minerals in the reactors were natural isotope-abundance ferrihydrite (^{NA}Fh), goethite (^{NA}Gt), or a mixture of both. The mixtures were prepared so that the percentages of Fe(III) coming from goethite were 5, 10, 15, 30, 40, 50, 60, or 70%. Reactors were crimp-sealed and placed on an orbital shaker at ∼23 °C in the absence of light. After 24 h, the bottles were manually shaken and opened, and all contents were filtered

https://doi.org/10.1021/acs.est.2c03925
Environ. Sci. Technol. 2022, 56, 12723−12733

using a syringe filter (0.22 μm, MCE membrane, MF-Millipore) and acidified to a concentration of 0.1 M HCl using 1 M HCl for subsequent Fe(II) and total Fe analysis using the phenanthroline method.

The solids collected on the filter were rinsed with 20 mL of degassed UPW and then dried in the glovebox until analysis with XRD. Duplicates were analyzed separately.

In our mineral mixture experiments, the ratio of ferrihydrite to goethite changed. Since ferrihydrite has a specific surface area considerably larger than goethite, there was a significant reduction of the overall specific surface area and possible higher sorption density of Fe(II) in experiments with smaller fractions of ferrihydrite. To investigate whether our results were influenced by a higher sorption density of Fe(II) onto ferrihydrite, we additionally prepared duplicate reactors comprising only ferrihydrite in which 5 mM of Fe(III) coming from ferrihydrite was reacted with 1 mM Fe(II), resulting in a higher Fe(II):Fe(III) ratio (1:5) than in the experiments described above (1:10 Fe(II):Fe(III) ratio). Other than the Fe(II):Fe(III) ratio, all other experimental conditions were kept constant.

Isotope Tracer Experiments. For a deeper understanding of ferrihydrite transformation in the presence of goethite, we employed an isotope tracer experiment in which ferrihydrite, goethite, and the aqueous Fe(II) were each labeled with different stable Fe isotopes (i.e., ^{54}Fe, ^{56}Fe, and ^{57}Fe). The isotopes were chosen so that exclusively one phase contained ^{57}Fe atoms in each reaction. We then used ^{57}Fe Mössbauer spectroscopy to analyze the solid phase, providing a unique snapshot of the fate of the ^{57}Fe atoms that originated as either ferrihydrite, goethite, or aqueous Fe(II). That, combined with the analyses of the isotopic composition of the aqueous phase and dissolved solids described below and XRD of the bulk solids, enabled us to gather information on how each of the Fe pools contributed to the overall reaction.

For the isotope tracer experiments, Fe(II) stock solutions for spiking were synthesized with the procedure described above, but with the ^{54}Fe isotope (Isoflex, 99.7% isotope purity) or ^{57}Fe isotope (Isoflex, 95.5% isotope purity). Reactions of Fe(II) with ferrihydrite or a 1:1 mixture of ferrihydrite and goethite (Fe(II)/Fe(III) ratio of 1:10) were repeated using a combination of isotope-labeled Fe(II) and minerals (details in Table S2). When we were following the ^{57}Fe from goethite or ferrihydrite, we used ^{NA}Fh or ^{NA}Gt (~2.3% ^{57}Fe, Table S1). However, since naturally abundant Fe also contains high concentrations of ^{56}Fe (~92% ^{56}Fe), we used ^{54}Fe(II) to trace Fe atoms originating in the aqueous phase. The use of ^{54}Fe(II) ensured that, in addition to tracing the ^{57}Fe in the solid phases using Mössbauer spectroscopy, we could also trace iron atoms initially in the aqueous Fe(II) and evaluate whether the system was moving toward complete isotope mixing between the solid and solution phases. All other experimental conditions described above were maintained. Experiments were run in duplicate. Fe(II) concentrations in the aqueous phase samples were analyzed using the 1,10-phenanthroline method,[46] and their Fe isotopic composition was determined via inductively coupled plasma-mass spectrometry (ICP-MS, Agilent 8800 Triple Quad) in reaction cell mode with an $H_{2(g)}$ flow rate of 7 mL min^{-1} to remove argide polyatomic interferences after diluting the samples to 50 ppb Fe, using previously established methods.[13] Fe isotopic composition results are reported as f^{X}Fe, being the counts of the isotope X divided by the sum of the counts of isotopes ^{54}Fe, ^{56}Fe, ^{57}Fe, and ^{58}Fe. The solid phases of the duplicates were combined for ^{57}Fe Mössbauer spectroscopy by collecting ~30 mg of solids from each duplicate on a filter membrane (0.22 μm, MCE membrane, MF-Millipore). The remaining solids from each duplicate were collected, rinsed with UPW, dried, and then combined for XRD analysis and determination of Fe isotopic composition after the solids were dissolved in 6 M HCl.

Electron Microscopy. The morphology of unreacted and reacted ferrihydrite, goethite, and a 1:1 mixture of both minerals were imaged with scanning transmission electron microscopy (STEM, HD2700Cs, Hitachi). For these analyses, ~2 mg of the washed solid phase was taken outside the glovebox, resuspended in 10 μL of UPW, drop-deposited onto a 200 mesh Cu grid coated with a holey C-coated support film (SPI supplies), and analyzed within 2 days. The microscope was operated at an acceleration voltage of 200 kV, and the signal of the secondary electron detector was used for image formation.

X-ray Diffraction and Quantitative Phase Analysis. Quantitative mineral phase analysis was performed by powder X-ray diffraction (XRD, D8 Advance, Bruker) using the Rietveld method. Samples were prepared in the glovebox by resuspending ~4 mg dried sample material in ethanol (~40 μL, Merck) and pipetting it onto a zero-background polished silicon wafer (Sil'tronix Silicon Technologies, France). The samples were measured in ambient air in Bragg–Brentano geometry using Cu Kα radiation (λ = 1.5418 Å, 40 kV and 40 mA) and a high-resolution energy-dispersive 1-D detector (LYNXEYE). Diffractograms were recorded from 10 to 70° 2θ with a step size of 0.02° 2θ and 10 s acquisition time per step. Rietveld quantitative phase analysis (QPA) was used to determine the relative contributions of mineral phases in diffraction patterns using TOPAS software (Version 5, Bruker AXS). Crystallite size was reported as the LVol-IB calculated in the TOPAS software. We included 2-line ferrihydrite as a mass-calibrated PONKCS (Partial Or No Known Crystal Structure) phase, as in some previous works.[6,11] In order to check that both ferrihydrite and goethite were quantifiable in mixtures based on the XRD patterns, we produced a series of goethite/ferrihydrite mixtures and quantified the individual mineral fractions based on XRD spectra using our fitting procedure (PONKCS method).[53] The absolute error between expected and fitted mineral fractions in these samples was ~12% (Figures S2 and S3). Therefore, differences smaller than that may be caused by uncertainties related to the fitting procedure rather than differences in the mineral fractions. We are aware that our goethite/ferrihydrite mixtures lack the complexity of the experimental samples to some extent, possibly resulting in higher uncertainties of the calculated minerals fractions of the experimental samples compared to our synthetic mixtures. Therefore, in addition to the mineral fractions obtained from fitting the XRD data using the PONKCS method, we also use trends observed over several samples to interpret our data.

^{57}Fe Mössbauer Spectroscopy. Solid samples were analyzed with Mössbauer spectroscopy at 77 and 4.2 K. Samples were prepared inside the glovebox by collecting solids on a filter membrane (0.22 μm, MCE membrane, MF-Millipore, ⌀ = 13 mm) and sealing it between two pieces of Kapton tape. We collected spectra in transmission mode using a constant acceleration drive system and a ^{57}Co source in a standard setup (WissEl, Wissenschaftliche Elektronik GmbH)

https://doi.org/10.1021/acs.est.2c03925
Environ. Sci. Technol. 2022, 56, 12723−12733

equipped with a closed-cycle cryostat (SHI-850, Janis Research Co.). The spectra were quantitatively interpreted using the software Recoil (University of Ottawa, Canada) by applying an extended Voigt-based fitting routine.[54] The velocity scale was calibrated using a 7 μm thick α-Fe(0) at room temperature. The half-width at half-maximum was fixed to 0.135 mm s^{-1}, the value of the inner line broadening of the calibration foil.

RESULTS AND DISCUSSION

Transformation of Ferrihydrite in the Absence or Presence of Goethite. To evaluate the influence of goethite on the transformation of ferrihydrite, we reacted ferrihydrite, goethite, or a 1:1 mixture of ferrihydrite and goethite with aqueous Fe(II). Quantitative XRD analysis showed that, after 24 h reaction with Fe(II), ferrihydrite was transformed to a mixture of ~59% ferrihydrite, ~22% goethite, and ~19% lepidocrocite (Figure 1a). In contrast, no mineral transformation or changes in the crystallite size were observed when goethite was reacted with Fe(II) (Figure 1b, Table S3). Based on these results, and assuming that the presence of goethite does not influence the transformation of ferrihydrite, one would expect that a 1:1 mixture of ferrihydrite and goethite would transform into ~30% ferrihydrite, ~61% goethite, and ~9% lepidocrocite. However, our experiment showed that this mixture transformed into ~2% ferrihydrite, ~ 91% goethite, and ~8% lepidocrocite (Figure 1c), suggesting that the presence of goethite promoted the transformation of ferrihydrite to goethite. Interestingly, the goethite formed via transformation of ferrihydrite in the pure ferrihydrite system had a larger estimated crystallite size (LVol-IB) than those of pure goethite that underwent recrystallization (Table S3). For the mixture of ferrihydrite and goethite, the interpretation of the crystallite size of reacted minerals is challenging because the initial goethite added to the systems accounts for a substantial mass of the final goethite and likely masks any changes.

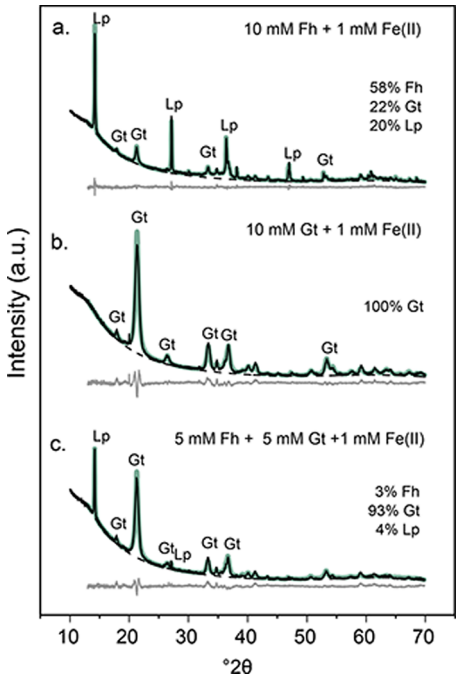

Figure 1. Rietveld quantitative phase analyses (QPA) for samples of (a) ferrihydrite, (b) goethite, or (c) a 1:1 mixture of ferrihydrite and goethite reacted with 1 mM Fe(II) for 24 h. Black lines show the measured XRD pattern, green lines show the Rietveld fit, lower gray line indicates model misfits, and dashed black lines show the background. Duplicates shown in Figure S4, data in Table S3. Abbreviations: Fh = ferrihydrite, Gt = goethite, and Lp = lepidocrocite.

To further investigate the influence of goethite on the transformation of ferrihydrite, we additionally reacted Fe(II) with mixtures of ferrihydrite and goethite in which the percentage of Fe(III) coming from goethite represented 5, 10, 15, 30, 40, 60, and 70%. The final mineral composition of the 24 h Fe(II)-reacted mineral mixtures is shown in Figure 2 (additional data in Figure S4 and Table S3), along with a "no-effect line" that illustrates expected contributions of transformation products assuming that the presence of goethite does not influence the transformation of ferrihydrite. Comparison between the observed data and the no-effect line revealed that for lepidocrocite measured data matched with the no-effect line. However, the transformation of ferrihydrite to goethite was promoted by the presence of goethite initially in the mixtures. This effect was clearly evident when the initial fraction of goethite was greater than 10%, suggesting that even small amounts of coexisting goethite can influence ferrihydrite transformation. While the quantification of low crystallinity phases using XRD is challenging, the differences between the "no-effect line" and the fitted values are much greater than the ~12% absolute error between expected and fitted values calculated in the quality control of the fits in this work (Figure S2) and similar work.[13] Calculations of the percentage of ferrihydrite in the initial mixtures that was transformed into goethite within 24 h (Figure 2d) showed that the more goethite that was initially present, the more ferrihydrite was transformed into goethite.

To test if the promoted formation of goethite resulted from a higher Fe(II) sorption density on the surface of ferrihydrite in mixtures with goethite (Figure S5), we additionally reacted pure ferrihydrite with aqueous Fe(II) at an Fe(II):Fe(III) ratio of 1:5 (compared to 1:10 in previous experiments). Despite the higher Fe(II) availability for sorption to ferrihydrite, similar net Fe(II) sorption density was observed (Table S2), and the 24 h reacted mineral phase comprised ~53% ferrihydrite, ~21% goethite, and ~26% lepidocrocite (Figure S6). These results are similar to those observed with pure ferrihydrite at a ratio of 1:10 (Figure 1a), with slightly more lepidocrocite formation in the reaction with 1:5 ratio. However, the higher Fe(II):Fe(III) ratio did not lead to the formation of more goethite. Therefore, the promoted formation of goethite in the mixtures was likely not caused by differences in the Fe(II) sorption density of ferrihydrite.

Morphology of the Transformation Products. Selected secondary electron (SE) images of the mineral phases before and after 24 h reaction with Fe(II) are shown in Figure 3. Additional images are provided in Figure S7. Unreacted ferrihydrite consisted of dense aggregates of ~0.4 μm (Figure 3a). Unreacted goethite (Figure 3c) formed microrods with ~0.5−1 μm length, similar to those synthesized by Cwiertny et al.[14] In the unreacted mixture of the minerals, ferrihydrite aggregates and goethite rods can be clearly distinguished, and both phases appeared in close contact with each other (Figure 3e).

Ferrihydrite reacted with Fe(II) was dominated by lepidocrocite platelets, star-like clusters of microrods forming radial twins representing goethite,[23] and small aggregates of

https://doi.org/10.1021/acs.est.2c03925
Environ. Sci. Technol. 2022, 56, 12723−12733

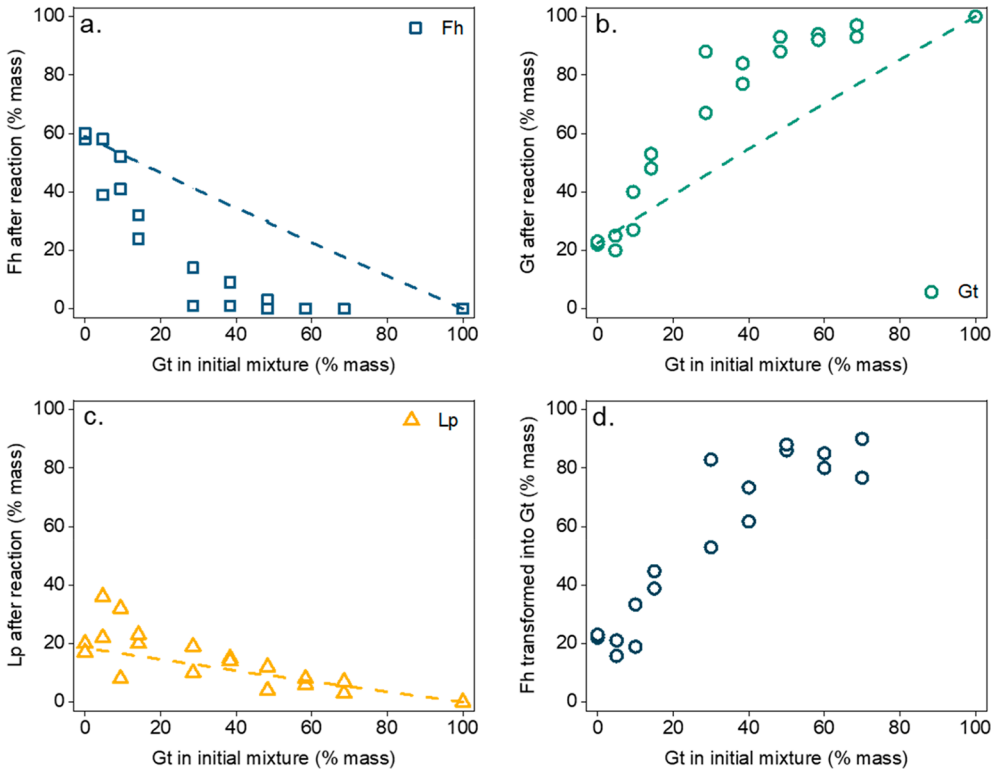

Figure 2. Mineral phase contributions for solids after 24 h reaction of Fe(II) with mixtures of ferrihydrite and goethite at different proportions. Panels a−c represent the effect in ferrihydrite, goethite, and lepidocrocite, respectively. Each marker corresponds to a different duplicate, and dashed lines represent the expected calculated values (no-effect lines). Panel d displays the percentage of ferrihydrite transformed into goethite when mixtures of ferrihydrite and goethite at different proportions reacted with 1 mM Fe(II) for 24 h. Note that the percentage of goethite in the *x*-axis is expressed in mass, according to values of Table S2. Abbreviations: Fh = ferrihydrite, Gt = goethite, and Lp = lepidocrocite.

ferrihydrite (Figures 3b and S7a), confirming the XRD findings of goethite and lepidocrocite as transformation products. In agreement with literature,[19] Fe(II)-reacted goethite did not display any substantial changes in morphology (Figures 3d and S7b). For the 1:1 mixture of ferrihydrite and goethite, the morphological changes upon reaction with Fe(II) are similar to the ones observed for ferrihydrite, with lepidocrocite platelets , star-like clusters of microrods forming radial twins representing goethite, and small aggregates of ferrihydrite (Figures 3f and S7c). In addition, SE images of the reacted mixture also revealed the abundance of goethite microrods (Figure S7c), including some large goethite rods near lepidocrocite and ferrihydrite (Figure 3f). However, through SE images alone, we cannot distinguish the goethite initially added to the reactor from the goethite newly formed by transformation of ferrihydrite. Moreover, we did not image or measure enough minerals to be able to make any statistically relevant claims regarding changes in the size of the particles.

In summary, the SE images of the mineral phases after 24 h reaction confirm the formation of goethite and lepidocrocite. They also indicate remaining ferrihydrite in samples of ferrihydrite and the 1:1 mixture of ferrihydrite and goethite reacted with Fe(II). Additionally, the results from STEM analyses demonstrated that the morphology of the phases formed upon reaction of ferrihydrite with Fe(II) are also formed in the 1:1 mixture of ferrihydrite and goethite reacted with Fe(II).

Understanding Transformation Pathways by Tracing Fe Pool Dynamics. For a deeper understanding of the mechanism of Fe(II)-catalyzed transformation of ferrihydrite in the presence of goethite, we repeated selected experiments and labeled the different Fe pools with different Fe isotopes. In each reaction, one phase (aqueous Fe(II), ferrihydrite, or goethite) was highly enriched in ^{57}Fe atoms (>95%). Therefore, mostly atoms originally in that phase are visible in the Mössbauer spectra of the reacted solids. The 4.2 K Mössbauer spectra of solids resulting from the reaction of ferrihydrite with Fe(II) are presented in Figure 4a,b, and the ones from the reaction of 1:1 mixture of ferrihydrite and goethite with Fe(II) are presented in Figure 4c−e.

For the reaction of aqueous Fe(II) with ferrihydrite alone, when the ^{57}Fe Mössbauer-active atoms were initially in the aqueous Fe(II), more than 95% of the signal registered in the Mössbauer spectrum came from atoms originally in the aqueous phase that were then incorporated into or adsorbed onto the solid phase (Figure 4a). The spectrum of the reacted solids collected at 4.2 K revealed two prominent sextets with parameters compatible with goethite (CS = 0.49 mm s^{-1}, QS = −0.08 mm s^{-1}, and H = 50.6 T)[20,48] and lepidocrocite (CS = 0.43 mm s^{-1}, QS = 0.01 mm s^{-1}, and H = 44.7 T).[48,49] Most features of the spectra could be reasonably fit with only those two phases (Fit 2, Figure S8 and Table S4), but since XRD patterns and EM images suggested the presence of ferrihydrite, we added a third sextet corresponding to ferrihydrite (Fit 1, Table S4). However, it is possible that the ferrihydrite seen using XRD and EM is not from the pool labeled with ^{57}Fe; therefore, we presented both fits. Since ferrihydrite and nanogoethite are challenging to differentiate using Mössbauer spectroscopy at 4.2 K, we fixed the parameters of the ferrihydrite sextet to match our initial synthesized ferrihydrite

https://doi.org/10.1021/acs.est.2c03925
Environ. Sci. Technol. 2022, 56, 12723−12733

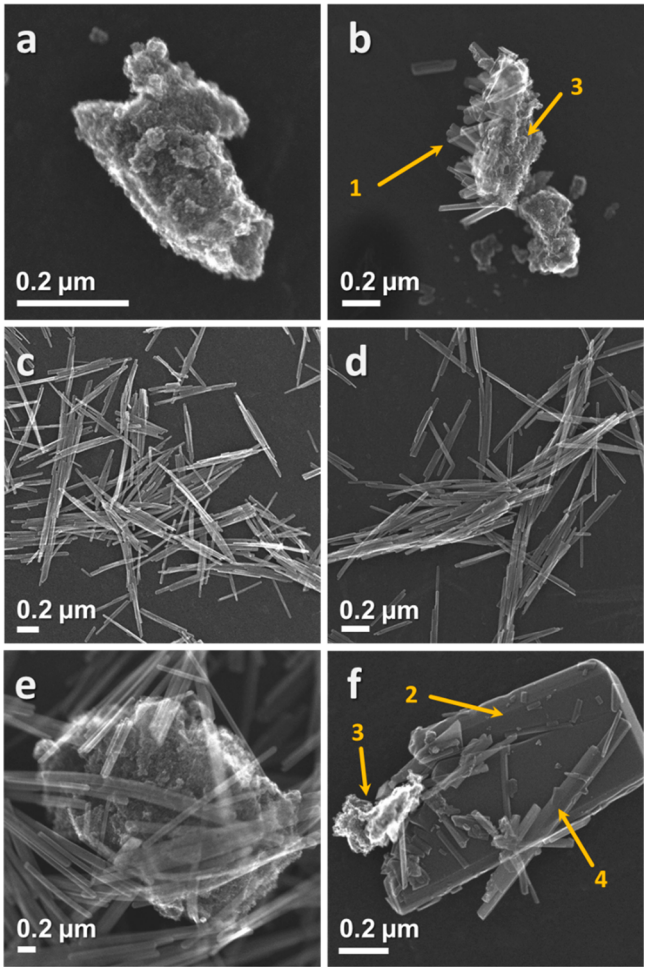

Figure 3. Secondary electron (SE) images of ferrihydrite, goethite, and mixture of ferrihydrite and goethite before (a, c, e, respectively) and after (b, d, f, respectively) reaction with 1 mM Fe(II) for 24 h. Arrows indicate goethite microrods (1), lepidocrocite platelets (2), aggregates of residual ferrihydrite (3), and large goethite rods (4).

(CS = 0.5 mm s^{-1}, QS = −0.01 mm s^{-1}, and H = 48.5 T) and only fitted the spectral area. To summarize the results, when Fe(II) reacts with ferrihydrite, the iron atoms originally at the aqueous phase formed 6% ferrihydrite, 14% goethite, and 80% lepidocrocite (Figure 4a). In contrast, when the ^{57}Fe atoms originated from ferrihydrite (>99% of the signal), 13% remained as ferrihydrite, 68% formed goethite, and 19% formed lepidocrocite (Figure 4b). The Mössbauer spectra collected at 77 K are presented in Figures S9 and, for the sample where the ^{57}Fe came from aqueous Fe(II) or ferrihydrite, presented a goethite sextet, a paramagnetic Fe(III) doublet, likely to be a mixture of ferrihydrite and lepidocrocite, in addition to a small collapsed feature, likely to be lepidocrocite undergoing magnetic ordering.[1,49,55,56]

For the reaction of ^{57}Fe(II) with a mixture of ferrihydrite and goethite, more than 95% of the signal of the 4.2 K Mössbauer spectra came from atoms originally in the aqueous phase that are now incorporated into or adsorbed onto the solid phase (Figure 4c). The atoms originally in the aqueous phase sorb to the solid phases and undergo electron transfer, forming in the solid phase 11% ferrihydrite, 31% goethite, and 57% lepidocrocite, in addition to 1% adsorbed Fe(II) (fitting parameters are detailed in Table S4). When the ^{57}Fe atoms were initially in ferrihydrite (>99% of the signal), the Mössbauer spectrum revealed the presence of the same Fe phases, with 9% of ^{57}Fe atoms remaining as ferrihydrite, 64% transformed into goethite, and 27% into lepidocrocite (Figure 4d). When the ^{57}Fe atoms were initially in goethite (>99% of the signal), most ^{57}Fe atoms remained as goethite, with the formation of 2% lepidocrocite (Figure 4e). The 77 K spectra of the samples containing ^{57}Fe initially in the aqueous phase or in ferrihydrite revealed a goethite sextet and a paramagnetic Fe(III) doublet, likely to be a mixture of ferrihydrite and lepidocrocite. Additionally, they contained a prominent collapsed sextet that possibly contains not only lepidocrocite but also a feature that orders into goethite parameters, likely to be nanogoethite or goethite with low crystallinity. For the sample containing ^{57}Fe initially in goethite, the 77 K spectrum was dominated by a goethite sextet with a small paramagnetic Fe(III) doublet of lepidocrocite.

To confirm that our results from the isotope tracer experiments were not affected by the use of minerals from different batches (which may have differed slightly in crystallinity, Figure S1), we also analyzed the solid phases with XRD (Figure S10). For ferrihydrite reacted with Fe(II) (average of two experiments), the transformation products comprised 54% ferrihydrite (standard deviation (SD) = 11), 13% (SD = 6) goethite, and 33% (SD = 17) lepidocrocite (compared to 59%, 22%, and 19%, respectively, for unlabeled experiments). The transformation products for the reactions of 1:1 mixture of ferrihydrite and goethite with Fe(II) (average of 3 experiments) comprised of 7% (SD = 9) ferrihydrite, 75% (SD = 12) goethite, and 18% (SD = 6) lepidocrocite (compared to 2%, 91%, and 8%, respectively, for unlabeled experiments). Despite the notable batch-to-batch differences, the overall conclusions remain the same as in our unlabeled experiment: when goethite is coexisting, more ferrihydrite turns into goethite.

To learn more about the fate of the Fe atoms in the aqueous and solid phases, we analyzed the Fe isotopic composition of the aqueous and solid phases before and after the reaction. Independent of the isotopes used, all systems moved toward isotopic mixing in 24 h reactions (Table S6 and Figure S11). While our data is limited to initial isotopic composition and one time point at 24 h, a closer look into the isotope data suggests that the main isotope used to trace the aqueous phase (either ^{54}Fe or ^{57}Fe) seems to have been incorporated into the solid phases to a greater extent in the mixture of ferrihydrite and goethite than in ferrihydrite by itself. Such an idea seems counterintuitive since goethite has a slower rate of Fe(II)−Fe(III) electron transfer than ferrihydrite.[6,7,32,34,36] It is possible that in the presence of goethite, more atoms form goethite, a mineral that likely has a slower turnover of its atoms through following rounds of Fe(II)−Fe(III) electron transfer.

Mechanism of Ferrihydrite Transformation. Characterization of Fe(II)-reacted ferrihydrite suggests that the mineral undergoes Fe(II)-catalyzed transformation and partially transforms into goethite and lepidocrocite in a 24 h reaction (Figure 1) as previously observed.[6,7,11,12,21,23] Previous works have investigated Fe(II)-catalyzed ferrihydrite transformation without the use of Fe isotopes as tracers or have used Mössbauer spectroscopy to observe either the aqueous phase[6] or the solid phase.[7,21] However, our approach of alternating the Fe pool containing the Mössbauer-active ^{57}Fe allowed us to further demonstrate that the atoms initially in the Fe(II) solution mostly form lepidocrocite (Figure 4a), while the atoms initially

https://doi.org/10.1021/acs.est.2c03925
Environ. Sci. Technol. 2022, 56, 12723−12733

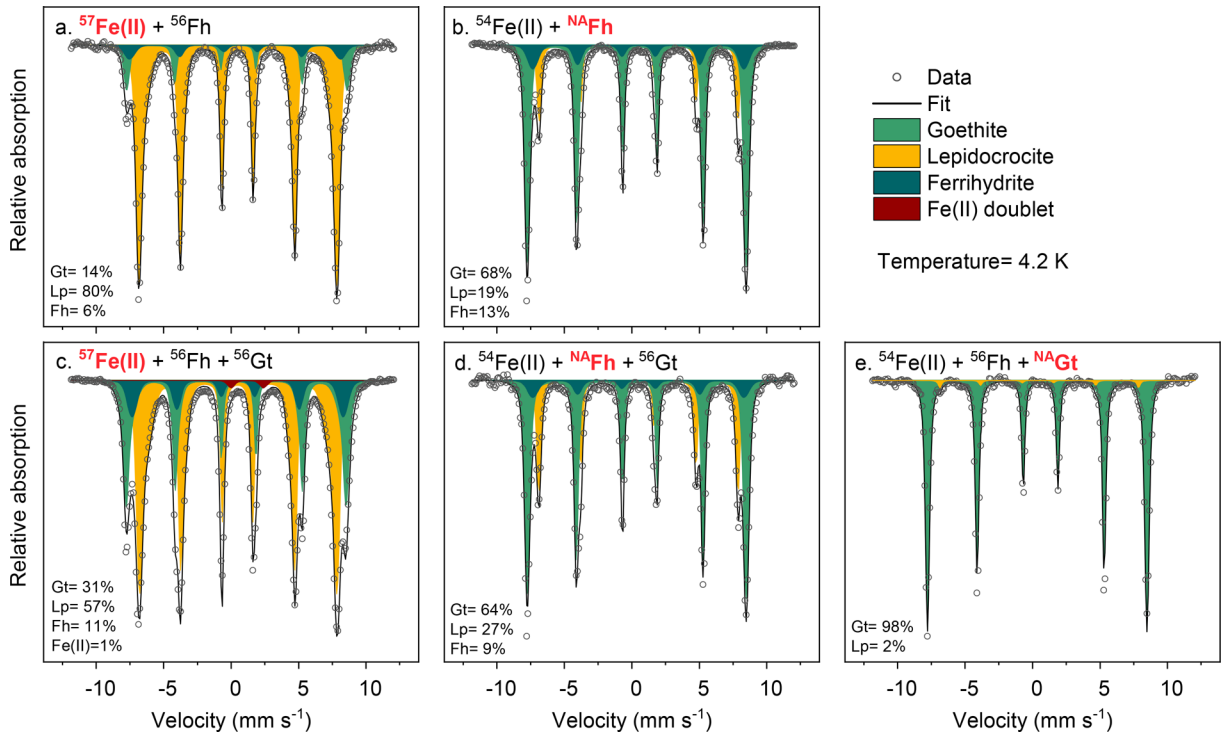

Figure 4. Mössbauer spectra of ferrihydrite (a and b) or a mixture of ferrihydrite and goethite (c–e) reacted with Fe(II). The phase highlighted in red is the phase that originally contained the ^{57}Fe atoms. The spectra were collected at 4.2 K. Abbreviations: Fh = ferrihydrite, Gt = goethite, and Lp = lepidocrocite.

in ferrihydrite mainly transform into goethite in 24 h (Figure 4b). We propose that the aqueous Fe(II) atoms that first sorb to ferrihydrite undergo Fe(II)–Fe(III) electron transfer, possibly inducing the growth of labile Fe(III),[21−23] which, under our experimental conditions, leads to the nucleation and growth of lepidocrocite. This mechanism is in alignment with frequent reports of lepidocrocite being the first mineral product observed during ferrihydrite transformation and with the recent microscopic evidence of a quasi-2D nanosheet of lepidocrocite that contours ferrihydrite during Fe(II)-catalyzed transformation.[23]

As for the Fe atoms from ferrihydrite preferentially forming goethite, previous works[9,23] and our EM images suggest that goethite precipitates were dominantly observed radiating outward from ferrihydrite aggregates (Figure 3b). We hypothesize that the constant reduction of Fe atoms from ferrihydrite caused by Fe(II)–Fe(III) electron transfer leads to a reorganization of Fe(III) in ferrihydrite at the atomic level that favors the formation of goethite nucleation sites. Alternatively, goethite formation may occur mostly in later stages of the experiment, when most of the Fe(II) initially in solution has already been oxidized to Fe(III) and incorporated into lepidocrocite, and Fe(II) in solution is then dominated by Fe atoms initially in ferrihydrite. Evidence of enrichment of the aqueous phase with Fe atoms initially in the solid phase has been previously reported.[6] Our isotope data is limited to a single time point at 24 h, when substantial isotope mixing has happened. Nonetheless, our results strongly suggest that the nature of the nucleation and growth of lepidocrocite and goethite lie in different mechanisms. The observation that Fe atoms from different Fe pools can preferentially form specific transformation products is a new finding that was only allowed due to our approach of alternating the Fe pool containing the Mössbauer-active ^{57}Fe.

Mechanism of Goethite Influence on Ferrihydrite Transformation. When pure goethite reacted with Fe(II) for 24 h, we observed no signs of mineral transformation (Figure 1a). These results were expected since crystalline minerals undergo Fe(II)-catalyzed recrystallization, with evidence of mixing between the atoms in the aqueous and solid phase but no mineral transformation.[28,31−34] For the 1:1 mixture of ferrihydrite and goethite reacted with Fe(II), we again observed the overall trend in which atoms from the aqueous phase mostly formed lepidocrocite while atoms from ferrihydrite formed goethite. However, a closer look at the data reveals that having goethite as a coexisting mineral adds or facilitates some mechanisms for mineral transformation.

The first mechanism is the formation of more goethite from the atoms initially in the aqueous phase. Our Mössbauer data shows that, in the absence of goethite, 14% of the iron atoms originating from the aqueous phase formed goethite, compared to 31% in the presence of goethite in the 1:1 mineral mixture (Figure 4). The enhanced formation of goethite from atoms in the aqueous phase in part results from the Fe(II)-goethite electron transfer of the atoms that sorbed onto goethite rather than ferrihydrite surfaces. In addition to the Mössbauer data, the isotopic composition of our isotope tracer experiment confirmed that Fe isotopes initially in goethite were found in the aqueous phase after 24 h, confirming that goethite recrystallization happened in the presence of ferrihydrite.[19,26,34] This is in agreement with several previous studies that have reported the formation of goethite from Fe(II) atoms that sorb onto goethite.[5,6,28,31,34]

The second and more intricate mechanism of goethite influence was observed with the atoms originally in

https://doi.org/10.1021/acs.est.2c03925
Environ. Sci. Technol. 2022, 56, 12723−12733

ferrihydrite. While the Mössbauer spectra collected at 4.2 K revealed that atoms initially in ferrihydrite transformed into similar amounts of goethite and lepidocrocite for the reactions in the presence or the absence of goethite (Figure 4d,b, respectively), the 77 K spectrum of the mineral mixture presented a large collapsed feature that was not a major component of the fits of the samples of ferrihydrite or goethite alone (Figure S9d,e). Such a collapsed sextet at 77 K that orders into goethite parameters at 4.2 K is likely to be nanogoethite.[57] Therefore, in the presence of goethite, atoms originally from ferrihydrite formed low-crystallinity goethite.

A current hypothesis to explain Fe(II)-catalyzed reduction of Fh is based on the formation of a labile Fe(III) that is more soluble than Fe(III) in ferrihydrite.[21,23,25,58] Building on this hypothesis, a possible explanation for the enhanced formation of goethite with low crystallinity in the presence of goethite reported in this study is that some of the labile Fe(III) was in close contact with the coexisting goethite, which serves as a readily available template for nanogoethite via template-directed nucleation. A similar mechanism was recently proposed to explain the formation of different end products from Fe(II)-catalyzed transformation of lepidocrocite in the presence of goethite.[58] In the Fe(II)-catalyzed transformation of ferrihydrite, the formation of a goethite nucleation site is an important step to drive the growth of transformation products,[9,22,58] but in the presence of coexisting goethite, the nucleation site is readily available and thus may accelerate the transformation of ferrihydrite into goethite. The formation of nanogoethite in the presence of coexisting goethite suggests this transformation pathway has thermodynamic advantages compared to the formation of goethite seen in systems of pure ferrihydrite, possibly due to size-driven thermodynamic differences among iron oxide phases.[59]

A third possible mechanism is that the oxidation of Fe(II) at the goethite surface might lead to electron transfer and hopping from goethite to closely associated ferrihydrite, leading to the accelerated dissolution of the ferrihydrite. While we have no direct evidence to prove this mechanism, electron hopping within ferrihydrite nanoparticles has been demonstrated,[60] and the proximity between ferrihydrite and goethite in our EM images supports such a hypothesis. This mechanism could explain why ferrihydrite exhibits accelerated dissolution to form more goethite in the presence of coexisting goethite. This would also explain the growth of goethite once goethite nucleation has occurred in systems of pure ferrihydrite reacted with Fe(II).

Environmental Implications. Our experiments demonstrated that the coexistence of goethite during Fe(II)-catalyzed transformation of ferrihydrite led to more transformation of ferrihydrite into goethite within a 24 h reaction time, likely through multiple mechanisms. The first mechanism is through the oxidation of Fe(II) at the surface of goethite instead of ferrihydrite, where the pre-existing goethite serves as a template for crystal growth. The second mechanism is template-directed nucleation and growth, in which labile Fe(III) formed via Fe(II)−Fe(III) electron transfer on ferrihydrite used the coexisting goethite as a readily available template for goethite nucleation and growth. We further hypothesize a third mechanism in which electrons transferred to goethite via oxidation of Fe(II) could undergo electron hopping to ferrihydrite, leading to the reductive dissolution of the latter phase. The produced aqueous Fe(II), which was initially in ferrihydrite, could then be oxidized again by goethite, thus feeding the growth of goethite crystals. Independent of the mechanism, soils and sediments likely contain multiple phases that influence each other's transformation pathways, especially in redox dynamic systems.

Quantifying how much the coexistence of goethite affects or accelerates the transformation of ferrihydrite is a challenging task. XRD suggests that, in a 24 h reaction with Fe(II), a 1:1 mixture of ferrihydrite and goethite have almost no ferrihydrite left, while for ferrihydrite itself, around 60% ferrihydrite would still be untransformed. While quantifying low crystallinity phases such as ferrihydrite and nanogoethite is challenging using XRD, such differences in ferrihydrite percentage are well beyond the associated errors. With Mössbauer spectroscopy, we learned that in the presence of goethite nanogoethite is formed, which is likely a more reactive and better sorbent phase than crystalline goethite formed via the transformation of ferrihydrite alone. By isolating each one of the Fe pools, our isotope tracer experiments demonstrated that upon reaction with Fe(II), the atoms originally in ferrihydrite mostly form goethite. In contrast, the atoms initially in the aqueous phase mostly form lepidocrocite. These results suggest that the mechanisms for goethite or lepidocrocite formation are likely different and depend not only on the supersaturation of the labile Fe(III) phase.[25] Additionally, the fate of the Fe atoms differs depending on the origin of the Fe atom (e.g., aqueous versus ferrihydrite versus goethite). Combined with the influence that coexisting Fe minerals have on overall transformation products, these factors will have critical importance for our understanding of the mechanisms that govern Fe(II)-catalyzed transformation of ferrihydrite and may further enhance our understanding of the release or sequestration of trace metals from Fe(III) minerals upon exposure to Fe(II).

The notion that coexisting minerals can drive mineral transformations into forming more of the same minerals might help explain the prevalence of goethite in soils and sediments, including records of goethite in younger redox dynamic soils.[61,62] From another perspective, ferrihydrite also changes the recrystallization of goethite, leading to the formation of nanogoethite, which is likely more reactive than goethite that underwent recrystallization by itself. Independent of the mechanism or nucleation pathway, the results of this study show that mineral transformations in natural soils and sediments, which contain multiple phases, are likely to be influenced by one another, especially in redox dynamic environments. Follow-up research should investigate if coexisting Fe minerals will affect the transformation of ferrihydrite in a soil matrix when an assemblage of particles is present.

Our findings might also be significant for the use of ferrihydrite in environmental applications. Ferrihydrite has been used in sand filters for the removals of arsenic from groundwater,[50,51] and it is also a common byproduct of permeable reactive barriers of zerovalent Fe.[52] When those filters and permeable reactive barriers are exposed to redox changes, the presence of goethite in the surrounding soils and materials might accelerate the transformation of ferrihydrite into goethite, possibly leading to a decrease in sorption capacity and reactivity. Future research should focus on the interface of ferrihydrite and soils to assess whether coexisting minerals affect ferrihydrite stability.

https://doi.org/10.1021/acs.est.2c03925
Environ. Sci. Technol. 2022, 56, 12723−12733

■ ASSOCIATED CONTENT

Supporting Information

The Supporting Information is available free of charge at https://pubs.acs.org/doi/10.1021/acs.est.2c03925.

Further details for material and methods and additional data and figures supporting the results (PDF)

■ AUTHOR INFORMATION

Corresponding Author

Luiza Notini − *Soil Chemistry Group, Institute of Biogeochemistry and Pollutant Dynamics, Department of Environmental Systems Science, ETH Zurich, CHN, CH-8092 Zurich, Switzerland;* orcid.org/0000-0003-2972-6588; Email: luiza.notini@usys.ethz.ch; Fax: +41 44 633 93 40

Authors

Laurel K. ThomasArrigo − *Soil Chemistry Group, Institute of Biogeochemistry and Pollutant Dynamics, Department of Environmental Systems Science, ETH Zurich, CHN, CH-8092 Zurich, Switzerland;* orcid.org/0000-0002-6758-3760

Ralf Kaegi − *Eawag, Swiss Federal Institute of Aquatic Science and Technology, CH-8600 Dübendorf, Switzerland;* orcid.org/0000-0002-2430-4733

Ruben Kretzschmar − *Soil Chemistry Group, Institute of Biogeochemistry and Pollutant Dynamics, Department of Environmental Systems Science, ETH Zurich, CHN, CH-8092 Zurich, Switzerland;* orcid.org/0000-0003-2587-2430

Complete contact information is available at: https://pubs.acs.org/10.1021/acs.est.2c03925

Notes

The authors declare no competing financial interest.

■ ACKNOWLEDGMENTS

We are grateful to Kurt Barmettler (ETH Zurich) for assisting with laboratory analyses. We further thank the three anonymous reviewers and the Associate Editor for their helpful comments, which significantly improved this manuscript. We acknowledge the Center for Optical and Electron Microscopy (ScopeM) of the ETH Zurich for providing access to their microscopes. This research is part of a project that has received funding from the European Research Council (ERC) under the European Union's Horizon 2020 research and innovation program (788009-IRMIDYN-ERC-2017-ADG).

■ REFERENCES

(1) Cornell, R. M.; Schwertmann, U. *The iron oxides: structure, properties, reactions, occurrences, and uses*; Wiley-VCH: Weinheim, 2003; Vol. 2.

(2) Childs, C. W. Ferrihydrite: a review of structure, properties and occurrence in relation to soils. *Z. Pflanz. Bodenkunde.* **1992**, *155* (5), 441−448.

(3) Lovley, D. R.; Phillips, E. J. Availability of ferric iron for microbial reduction in bottom sediments of the freshwater tidal potomac river. *Appl. Environ. Microbiol.* **1986**, *52* (4), 751−757.

(4) van der Zee, C.; Roberts, D. R.; Rancourt, D. G.; Slomp, C. P. Nanogoethite is the dominant reactive oxyhydroxide phase in lake and marine sediments. *Geology* **2003**, *31* (11), 993−996.

(5) Williams, A. G. B.; Scherer, M. M. Spectroscopic evidence for Fe(II)−Fe(III) electron transfer at the iron oxide−water interface. *Environ. Sci. Technol.* **2004**, *38* (18), 4782−4790.

(6) ThomasArrigo, L. K.; Byrne, J. M.; Kappler, A.; Kretzschmar, R. Impact of organic matter on iron(II)-catalyzed mineral transformations in ferrihydrite−organic matter coprecipitates. *Environ. Sci. Technol.* **2018**, *52* (21), 12316−12326.

(7) Zhou, Z.; Latta, D. E.; Noor, N.; Thompson, A.; Borch, T.; Scherer, M. M. Fe(II)-catalyzed transformation of organic matter−ferrihydrite coprecipitates: a closer look using Fe isotopes. *Environ. Sci. Technol.* **2018**, *52* (19), 11142−11150.

(8) Chen, C.; Kukkadapu, R.; Sparks, D. L. Influence of coprecipitated organic matter on $Fe^{2+(aq)}$-catalyzed transformation of ferrihydrite: implications for carbon dynamics. *Environ. Sci. Technol.* **2015**, *49* (18), 10927−10936.

(9) Hansel, C. M.; Benner, S. G.; Fendorf, S. Competing Fe(II)-induced mineralization pathways of ferrihydrite. *Environ. Sci. Technol.* **2005**, *39* (18), 7147−7153.

(10) Hiemstra, T.; Mendez, J. C.; Li, J. Evolution of the reactive surface area of ferrihydrite: time, pH, and temperature dependency of growth by Ostwald ripening. *Environ. Sci. Nano* **2019**, *6* (3), 820−833.

(11) ThomasArrigo, L. K.; Kaegi, R.; Kretzschmar, R. Ferrihydrite growth and transformation in the presence of ferrous iron and model organic ligands. *Environ. Sci. Technol.* **2019**, *53* (23), 13636−13647.

(12) Zhou, Z.; Muehe, E. M.; Tomaszewski, E. J.; Lezama-Pacheco, J.; Kappler, A.; Byrne, J. M. Effect of natural organic matter on the fate of cadmium during microbial ferrihydrite reduction. *Environ. Sci. Technol.* **2020**, *54* (15), 9445−9453.

(13) Schulz, K.; ThomasArrigo, L. K.; Kaegi, R.; Kretzschmar, R. Stabilization of ferrihydrite and lepidocrocite by silicate during Fe(II)-catalyzed mineral transformation: impact on particle morphology and silicate distribution. *Environ. Sci. Technol.* **2022**, *56* (9), 5929−5938.

(14) Cwiertny, D. M.; Handler, R. M.; Schaefer, M. V.; Grassian, V. H.; Scherer, M. M. Interpreting nanoscale size-effects in aggregated Fe-oxide suspensions: reaction of Fe(II) with goethite. *Geochim. Cosmochim. Acta* **2008**, *72* (5), 1365−1380.

(15) Mitsunobu, S.; Muramatsu, C.; Watanabe, K.; Sakata, M. Behavior of antimony(V) during the transformation of Ferrihydrite and Its environmental implications. *Environ. Sci. Technol.* **2013**, *47* (17), 9660−9667.

(16) Zhou, Z.; Latta, D. E.; Scherer, M. M. Natural organic matter inhibits Ni stabilization during Fe(II)-catalyzed ferrihydrite transformation. *Sci. Total Environ.* **2021**, *755*, 142612.

(17) Fei, Y.; Hua, J.; Liu, C.; Li, F.; Zhu, Z.; Xiao, T.; Chen, M.; Gao, T.; Wei, Z.; Hao, L. Aqueous Fe(II)-induced phase transformation of ferrihydrite coupled adsorption/immobilization of rare earth elements. *Minerals* **2018**, *8* (8), 357.

(18) Kukkadapu, R. K.; Zachara, J. M.; Fredrickson, J. K.; Smith, S. C.; Dohnalkova, A. C.; Russell, C. K. Transformation of 2-line ferrihydrite to 6-line ferrihydrite under oxic and anoxic conditions. *Am. Mineral.* **2003**, *88* (11−12), 1903−1914.

(19) Handler, R. M.; Beard, B. L.; Johnson, C. M.; Scherer, M. M. Atom exchange between aqueous Fe(II) and goethite: an Fe isotope tracer study. *Environ. Sci. Technol.* **2009**, *43* (4), 1102−1107.

(20) Byrne, J. M.; Kappler, A. Mössbauer spectroscopy. In *Analytical Geomicrobiology: A Handbook of Instrumental Techniques*; Alessi, D. S.; Veeramani, H.; Kenney, J. P. L., Eds.;Cambridge University Press: 2019

(21) Sheng, A.; Liu, J.; Li, X.; Qafoku, O.; Collins, R. N.; Jones, A. M.; Pearce, C. I.; Wang, C.; Ni, J.; Lu, A.; Rosso, K. M. Labile Fe(III) from sorbed Fe(II) oxidation is the key intermediate in Fe(II)-catalyzed ferrihydrite transformation. *Geochim. Cosmochim. Acta* **2020**, *272*, 105−120.

(22) Boland, D. D.; Collins, R. N.; Miller, C. J.; Glover, C. J.; Waite, T. D. Effect of solution and solid-phase conditions on the Fe(II)-accelerated transformation of ferrihydrite to lepidocrocite and goethite. *Environ. Sci. Technol.* **2014**, *48* (10), 5477−5485.

(23) Qafoku, O.; Kovarik, L.; Bowden, M. E.; Nakouzi, E.; Sheng, A.; Liu, J.; Pearce, C. I.; Rosso, K. M. Nanoscale observations of

Fe(II)-induced ferrihydrite transformation. *Environ. Sci. Nano* **2020**, *7* (10), 2953−2967.
(24) Gomez, M. A.; Jiang, R.; Song, M.; Li, D.; Lea, A. S.; Ma, X.; Wang, H.; Yin, X.; Wang, S.; Jia, Y. Further insights into the Fe(II) reduction of 2-line ferrihydrite: a semi in situ and in situ TEM study. *Nanoscale Adv.* **2020**, *2* (10), 4938−4950.
(25) Sheng, A.; Liu, J.; Li, X.; Luo, L.; Ding, Y.; Chen, C.; Zhang, X.; Wang, C.; Rosso, K. M. Labile Fe(III) supersaturation controls nucleation and properties of product phases from Fe(II)-catalyzed ferrihydrite transformation. *Geochim. Cosmochim. Acta* **2021**, *309*, 272−285.
(26) Handler, R. M.; Frierdich, A. J.; Johnson, C. M.; Rosso, K. M.; Beard, B. L.; Wang, C.; Latta, D. E.; Neumann, A.; Pasakarnis, T.; Premaratne, W. A. P. J.; Scherer, M. M. Fe(II)-catalyzed recrystallization of goethite revisited. *Environ. Sci. Technol.* **2014**, *48* (19), 11302−11311.
(27) Taylor, S. D.; Liu, J.; Zhang, X.; Arey, B. W.; Kovarik, L.; Schreiber, D. K.; Perea, D. E.; Rosso, K. M. Visualizing the iron atom exchange front in the Fe(II)-catalyzed recrystallization of goethite by atom probe tomography. *Proc. Natl. Acad. Sci. U. S. A.* **2019**, *116* (8), 2866−2874.
(28) Notini, L.; Latta, D. E.; Neumann, A.; Pearce, C. I.; Sassi, M.; N'Diaye, A. T.; Rosso, K. M.; Scherer, M. M. The role of defects in Fe(II)−goethite electron transfer. *Environ. Sci. Technol.* **2018**, *52* (5), 2751−2759.
(29) Alexandrov, V.; Rosso, K. M. Ab initio modeling of Fe(II) adsorption and interfacial electron transfer at goethite (α-FeOOH) surfaces. *Phys. Chem. Chem. Phys.* **2015**, *17* (22), 14518−14531.
(30) Zarzycki, P.; Rosso, K. M. Energetics and the role of defects in Fe(II)-catalyzed goethite recrystallization from molecular simulations. *ACS Earth Space Chem.* **2019**, *3* (2), 262−272.
(31) Notini, L.; Latta, D. E.; Neumann, A.; Pearce, C. I.; Sassi, M.; N'Diaye, A. T.; Rosso, K. M.; Scherer, M. M. A closer look at Fe(II) passivation of goethite. *ACS Earth Space Chem.* **2019**, *3* (12), 2717−2725.
(32) Joshi, P.; Fantle, M. S.; Larese-Casanova, P.; Gorski, C. A. Susceptibility of goethite to Fe^{2+}-catalyzed recrystallization over time. *Environ. Sci. Technol.* **2017**, *51* (20), 11681−11691.
(33) Pasakarnis, T.; McCormick, M. L.; Parkin, G. F.; Thompson, A.; Scherer, M. M. $Fe(II)_{aq}$−$Fe(III)_{oxide}$ electron transfer and Fe exchange: effect of organic carbon. *Environ. Chem.* **2015**, *12* (1), 52−63.
(34) Latta, D. E.; Bachman, J. E.; Scherer, M. M. Fe electron transfer and atom exchange in goethite: influence of Al-substitution and anion sorption. *Environ. Sci. Technol.* **2012**, *46* (19), 10614−10623.
(35) Joshi, P.; Gorski, C. A. Anisotropic morphological changes in goethite during Fe^{2+}-catalyzed recrystallization. *Environ. Sci. Technol.* **2016**, *50* (14), 7315−7324.
(36) Southall, S. C.; Micklethwaite, S.; Wilson, S. A.; Frierdich, A. J. Changes in crystallinity and tracer-isotope distribution of goethite during Fe(II)-accelerated recrystallization. *ACS Earth Space Chem.* **2018**, *2* (12), 1271−1282.
(37) Aeppli, M.; Voegelin, A.; Gorski, C. A.; Hofstetter, T. B.; Sander, M. Mediated Electrochemical Reduction of Iron (Oxyhydr-)Oxides under Defined Thermodynamic Boundary Conditions. *Environ. Sci. Technol.* **2018**, *52* (2), 560−570.
(38) Aeppli, M.; Kaegi, R.; Kretzschmar, R.; Voegelin, A.; Hofstetter, T. B.; Sander, M. Electrochemical Analysis of Changes in Iron Oxide Reducibility during Abiotic Ferrihydrite Transformation into Goethite and Magnetite. *Environ. Sci. Technol.* **2019**, *53* (7), 3568−3578.
(39) Buchholz, A.; Laskov, C.; Haderlein, S. B. Effects of Zwitterionic Buffers on Sorption of Ferrous Iron at Goethite and Its Oxidation by CCl4. *Environ. Sci. Technol.* **2011**, *45* (8), 3355−3360.
(40) ThomasArrigo, L. K.; Notini, L.; Shuster, J.; Nydegger, T.; Vontobel, S.; Fischer, S.; Kappler, A.; Kretzschmar, R. Mineral characterization and composition of Fe-rich flocs from wetlands of Iceland: Implications for Fe, C and trace element export. *Sci. Total Environ.* **2022**, *816*, 151567.
(41) Regelink, I. C.; Voegelin, A.; Weng, L.; Koopmans, G. F.; Comans, R. N. J. Characterization of colloidal Fe from soils using field-flow fractionation and Fe K-edge X-ray absorption spectroscopy. *Environ. Sci. Technol.* **2014**, *48* (8), 4307−4316.
(42) Vodyanitskii, Y. N.; Sivtsov, A. Formation of ferrihydrite, ferroxyhyte, and vernadite in soil. *Eurasian Soil Sci.* **2004**, *37* (8), 863−875.
(43) Amstaetter, K.; Borch, T.; Larese-Casanova, P.; Kappler, A. Redox Transformation of Arsenic by Fe(II)-Activated Goethite (α-FeOOH). *Environ. Sci. Technol.* **2010**, *44* (1), 102−108.
(44) Gorski, C. A.; Scherer, M. M. Influence of Magnetite Stoichiometry on Fe^{II} Uptake and Nitrobenzene Reduction. *Environ. Sci. Technol.* **2009**, *43* (10), 3675−3680.
(45) Larese-Casanova, P.; Scherer, M. M. Fe(II) Sorption on Hematite: New Insights Based on Spectroscopic Measurements. *Environ. Sci. Technol.* **2007**, *41* (2), 471−477.
(46) Tamura, H.; Goto, K.; Yotsuyanagi, T.; Nagayama, M. Spectrophotometric determination of iron(II) with 1,10-phenanthroline in the presence of large amounts of iron(III). *Talanta* **1974**, *21* (4), 314−318.
(47) Cwiertny, D. M.; Handler, R. M.; Schaefer, M. V.; Grassian, V. H.; Scherer, M. M. Interpreting nanoscale size-effects in aggregated Fe-oxide suspensions: reaction of Fe(II) with goethite. *Geochim. Cosmochim. Acta* **2008**, *72* (5), 1365−1380.
(48) Byrne, J. M.; Kappler, A. Mössbauer spectroscopy. In *Analytical Geomicrobiology: A Handbook of Instrumental Techniques*; Alessi, D. S., Veeramani, H., Kenney, J. P. L., Eds.; Cambridge University Press: Cambridge, 2019; pp 314−338.
(49) Vandenberghe, R. E.; De Grave, E. Application of Mössbauer spectroscopy in earth sciences. In *Mössbauer Spectroscopy: Tutorial Book*; Yoshida, Y., Langouche, G., Eds.; Springer: Berlin, Heidelberg, 2013; pp 91−185.
(50) Jessen, S.; Larsen, F.; Koch, C. B.; Arvin, E. Sorption and Desorption of Arsenic to Ferrihydrite in a Sand Filter. *Environ. Sci. Technol.* **2005**, *39* (20), 8045−8051.
(51) Bretzler, A.; Nikiema, J.; Lalanne, F.; Hoffmann, L.; Biswakarma, J.; Siebenaller, L.; Demange, D.; Schirmer, M.; Hug, S. J. Arsenic removal with zero-valent iron filters in Burkina Faso: Field and laboratory insights. *Sci. Total Environ.* **2020**, *737*, 139466.
(52) Furukawa, Y.; Kim, J.-w.; Watkins, J.; Wilkin, R. T. Formation of Ferrihydrite and Associated Iron Corrosion Products in Permeable Reactive Barriers of Zero-Valent Iron. *Environ. Sci. Technol.* **2002**, *36* (24), 5469−5475.
(53) Scarlett, N. V. Y.; Madsen, I. C. Quantification of phases with partial or no known crystal structures. *Powder Diffr.* **2006**, *21* (4), 278−284.
(54) Lagarec, K.; Rancourt, D. G. Extended Voigt-based analytic lineshape method for determining N-dimensional correlated hyperfine parameter distributions in Mössbauer spectroscopy. *Nucl. Instrum. Methods Phys. Res. B* **1997**, *129* (2), 266−280.
(55) Murad, E.; Cashion, J. Mössbauer spectroscopy of environmental materials and their industrial utilization. Springer Science & Business Media: 2011
(56) Cornell, R. M.; Schwertmann, U. The iron oxides: structure, properties, reactions, occurrences, and uses. Wiley-vch Weinheim: 2003 Vol.2
(57) Thompson, A.; Chadwick, O. A.; Rancourt, D. G.; Chorover, J. Iron-oxide crystallinity increases during soil redox oscillations. *Geochim. Cosmochim. Acta* **2006**, *70* (7), 1710−1727.
(58) Liu, J.; Sheng, A.; Li, X.; Arai, Y.; Ding, Y.; Nie, M.; et al. Understanding the importance of labile Fe(III) during Fe(II)-catalyzed transformation of metastable iron oxyhydroxides. *Environ. Sci. Technol.* **2022**, *56* (6), 3801−3811.
(59) Navrotsky, A.; Mazeina, L.; Majzlan, J. Size-driven structural and thermodynamic complexity in iron oxides. *Science* **2008**, *319* (5870), 1635−1638.
(60) Soltis, J. A.; Schwartzberg, A. M.; Zarzycki, P.; Penn, R. L.; Rosso, K. M.; Gilbert, B. Electron mobility and trapping in ferrihydrite nanoparticles. *ACS Earth Space Chem.* **2017**, *1* (4), 216−226.

https://doi.org/10.1021/acs.est.2c03925
Environ. Sci. Technol. 2022, 56, 12723−12733

(61) Tamura, T.; Jackson, M. L.; Sherman, G. D. Mineral Content of Low Humic, Humic and Hydrol Humic Latosols of Hawaii. *Soil Sci. Soc. Am. J.* **1953**, *17* (4), 343−346.
(62) Wada, K.; Wada, S.-I. Clay mineralogy of the B horizons of two hydrandepts, a Torrox and a Humitropept in Hawaii. *Geoderma* **1976**, *16* (2), 139−157.

https://doi.org/10.1021/acs.est.2c03925
Environ. Sci. Technol. 2022, 56, 12723−12733